Numerical study of a very intensive eastern Mediterranean dust storm, 13–16 March 1998

M. Tsidulko,[1] S. O. Krichak, and P. Alpert

Department of Geophysics and Planetary Sciences, Raymond and Beverly Sackler Faculty of Exact Sciences, Tel Aviv University, Israel

O. Kakaliagou, G. Kallos, and A. Papadopoulos

Department of Applied Physics, University of Athens, Greece

Received 30 July 2001; revised 10 December 2001; accepted 25 July 2002; published XX Month 2002.

[1] Presented herein is an analysis of an exceptionally intensive central and eastern Mediterranean dust intrusion of 15–16 March, 1998. The intrusion has been associated with development of an intense cyclone over Africa. The weather and dust development processes were simulated with the Eta weather and dust prediction model. Also presented is a comparison of the model results with the Total Ozone Mass Spectrometer Aerosol Index (TOMS AI) pictures as well as with those of the surface and weather observations. The roles of the main processes responsible for the dust plume development and associated dust intrusion to the eastern Mediterranean (EM) are studied. The observation data as well as the model-simulated parameters are jointly analyzed. The analysis also includes the data from the back-trajectory computations. With the aid of the model-produced dust profiles we studied the significant variation in the altitudes of the dust layers within the cyclone sectors. In the warm sector of the cyclone located over the Mediterranean Sea the dust layer extended up to 8–10 km. Relatively low dust concentration values were found here. In the area of the cold front over Africa the dust was restricted to the lower troposphere and the planetary boundary layer. Here the model simulated high values of the dust concentrations. The sharp TOMS AI increase over Israel and the eastern Mediterranean up to 5.0 units, further away from the dust sources, is explained by the strong winds, by the increased cyclone convergence, and the formation of a two-layer dust plume. *INDEX TERMS:* 3360 Meteorology and Atmospheric Dynamics: Remote sensing; 0305 Atmospheric Composition and Structure: Aerosols and particles (0345, 4801); 3329 Meteorology and Atmospheric Dynamics: Mesoscale meteorology; *KEYWORDS:* dust storm, dust plume, cyclone, Mediterranean, eta model, TOMS AI

Citation: Tsidulko, M., S. O. Krichak, P. Alpert, O. Kakaliagou, G. Kallos, and A. Papadopoulos, Numerical study of a very intensive eastern Mediterranean dust storm, 13–16 March 1998, *J. Geophys. Res.*, *107*(0), XXXX, doi:10.1029/2001JD001168, 2002.

1. Introduction

[2] On March 16, 1998, the eastern Mediterranean (EM) region experienced an exceptionally intensive dust outbreak. According to the Israeli surface measurements, concentration of the respirable size dust particles at 10 m height reached 8000 $\mu g\ m^{-3}$ at 0600 LT March 16 [*Alpert and Ganor*, 2001]. Aerosol Index (AI) images from the Total Ozone Mass Spectrometer (TOMS) satellite [*Hsu et al.*, 1999] showed high (more than 5.0 AI units) values at about 1100 LT on that day, over the whole EM region.

[3] The large and dense aerosol plume has been transported to the area from Northern Africa. As demonstrated by *Alpert and Ganor* [2001], the intrusion was associated with the development of an intensive Northern African cyclone. The cyclone-related mesoscale frontlines and associated strong winds could have triggered the intensive dust updraft on the cyclone's route over Northern Africa to Israel. This cannot explain, however, the unusually high dust concentration over the EM. A deeper understanding of the mechanisms responsible for the dust plume intensity is required.

[4] The mineral dust forecasting is a relatively new area of application of the hydrodynamic modeling approach. First, modeling experiments by *Westphal et al.* [1987], *Marticorena and Bergametti* [1995], and *Nickovic and Dobricic* [1996] may be referenced. The importance of the accurate description of the aerosol effects in the weather prediction and, especially, in climate models has been underestimated until the last decade. The lack of interest regarding the subject was mainly associated with the absence of observation data. No fully reliable data on the

[1]Now at NOAA Coast Survey Development Laboratory, Silver Spring, Maryland, USA.

Copyright 2002 by the American Geophysical Union.
0148-0227/02/2001JD001168$09.00

distribution of the dust sources was available either. The situation is improving now, with the implementation of new observation systems aboard the satellites and a deeper analysis of the data from the already existing platforms. All this is associated to the overall progress in atmospheric and, especially, climate modeling. The role of the dust effects in the climatic developments appears to be quite significant [*Alpert et al.*, 1998; *Cautenet et al.*, 1992; *Podgorny et al.*, 2000; *Rosenfeld et al.*, 2001].

[5] The development of new, more accurate dust prediction models enables forecasters to apply their products in daily use. Comparison of the model predictions of the surface dust concentration with the observations (available for verification mainly over the populated areas) demonstrates a good level of reliability of the forecasts. The model-produced patterns with the vertically integrated dust content in the atmosphere (dust loading) are also in good agreement with the available satellite data [*Alpert et al.*, 2002]. This allows application of the results of successful dust simulations as additional information for the analysis. The approach was adapted in the study.

[6] The case [*Alpert and Ganor*, 2001] has been characterized by unusually high values of dust concentration (8000 $\mu g\ m^{-3}$) over the EM area. The physical mechanisms responsible for the rapid increase of the dust concentration from March 14 to March 16 are not fully understood. Several explanations are possible. The high values of the observed surface dust concentration in Tel Aviv [*Alpert and Ganor*, 2001] support explanation associated with the dust plume transport. The mechanism of formation of the unusually dense dust plume is not clear, since the EM area is located too far away from the dust source area. A different explanation is also possible: The observed AI increase over the EM up to the value of 5.0 units, which is unusual for the region, could be associated with a dust updraft, due to a higher sensitivity of the TOMS AI computation procedure to the dust at higher levels [*Hsu et al.*, 1999].

2. Weather and Dust Prediction Model

[7] The Eta weather and dust prediction model has been adapted at Tel Aviv University with the help of the University of Athens's group [*Krichak et al.*, 1999]. The model has already been discussed in detail [*Mesinger*, 1996]. The dust package is described by *Nickovic et al.* [1997a, 1997b] and *Kallos et al.* [1997]. The following main characteristics of the system may be indicated.

2.1. Dynamics and Numerics

[8] A hydrostatic Eta/NCEP sigma-eta vertical coordinate model [*Mesinger et al.*, 1988; *Janjic*, 1990; *Mesinger*, 1996] is used. The configured model domain covers the area 15°E–45°E, 15°N–45°N with horizontal resolution of 0.5°. Arakawa E-grid in the horizontal plane and vertical eta coordinate, with the step-like silhouette topography is adapted. The model atmosphere contains 32 vertical levels. The model's finite difference approximation secures conservation of finite difference analogs of chosen integral constrains of the continuous atmosphere and minimization of spurious departures from the physical system, computational modes and false instabilities. Computation of the horizontal advection of passive substances (including dust concentration) is performed according to the conservative positive-definite scheme [*Janjic*, 1994].

2.2. Dust Parameterization

[9] The dust prediction module includes parameterization of mobilization, transport, and wet/dry deposition effects. The corresponding parameterization schemes are discussed by *Nickovic and Dobricic* [1996], *Nickovic et al.* [1997a, 1997b] and *Kallos et al.* [1997]. All of the dust (clay) particles in the model are assumed to be of the same size (effective radius of 2–2.5 microns). The dust is considered as a passive substance. Computation of the relative vertical velocity of the dust particles is performed according to the vertical air velocity and the gravitational settling velocity, derived from the Stokes formula. The dust mobilization scheme takes into account the values of the friction- and threshold friction velocity, soil wetness and the distribution of the dust source areas, which are specified according to the *Olson et al.* [1985] vegetation type data set. The set contains 59 classes of vegetation with 10′ resolution. Only the desert and semi-desert areas are assumed to contain the dust sources [*Nickovic et al.*, 1997a, 1997b]. This approximation is not the only possible one. According to the assumption a large area over Northern Africa is considered as the dust source one. This contradicts with the recent results by *Prospero et al.* [2002], according to which the dust source areas are mainly found in the topographic lows. An example of the application of a more accurate approach for the dust source area determination is given by *Alpert et al.* [2002].

2.3. Physics

[10] The land-surface parameterization is performed according to *Chen et al.* [1997]. The model employs the planetary boundary layer parameterization according to the Monin-Obukhov similarity theory with the use of the Mellor-Yamada Level 2 model [*Janjic*, 1994; *Mesinger*, 1996]. It also employs the viscous sublayer [*Janjic*, 1994; *Zilitinkevich*, 1995] approach over land and water, respectively. Cumulus parameterization is performed according to the Betts-Miller-Janjic [*Betts*, 1986; *Janjic*, 1994] deep and shallow moist-convection scheme. In case of instability, temperature and moisture are adjusted here to empirical reference profiles. Short- and long-wave radiation processes (without the aerosol feedback effects) are parameterized according to *Lacis and Hansen* [1974] and *Fels and Shwartzkopf* [1975], respectively. The fact that the dust effects are not included in the radiation transfer calculations may lead to an underestimation of the radiation heating inside (and a cooling below) a dense dust layer and the corresponding lapse rate changes [*Alpert et al.*, 1998; *Podgorny et al.*, 2000].

3. Data and Organization of the Experiment

[11] The aim of the study was to simulate the unusually intensive Saharan dust intrusion to the EM and to analyze the involved processes using both the observations and the model-produced data. Objective analysis data of the European Center for Medium Range Weather Forecasts (ECMWF) were adapted in the simulation run. The data are for the period between 1200 UTC March 13 and 1200 UTC March

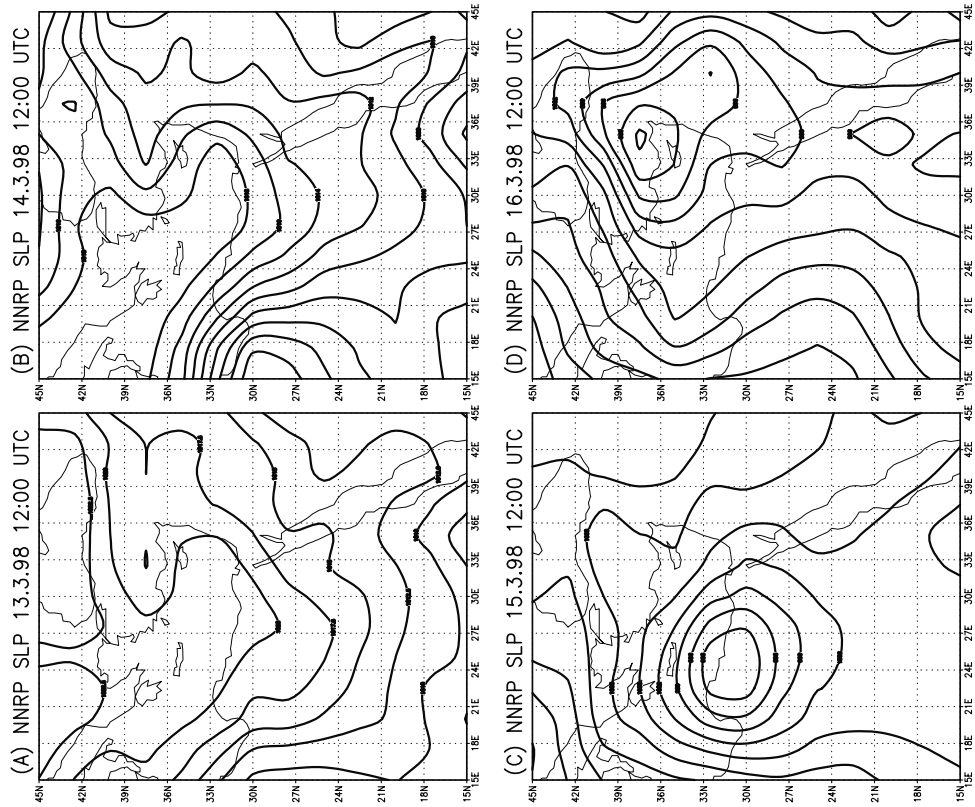

Figure 1. NNRP based SLP patterns (hPa) at 1200 UTC of (a) 13 March, (b) 14 March, (c) 15 March, and (d) 16 March 1998. Contour interval is 2.5 hPa.

17, 1998, available with 6-hour time intervals and a 0.5° horizontal resolution, and determined at 11 isobaric surfaces: 1000, 950, 850, 700, 600, 500, 400, 300, 250, 200, 150, and 100 hPa.

[12] Updated sets of the ECMWF data on the meteorological parameters are used for each of the 24-hour runs. The procedure used for the dust initialization [*Nickovic et al.*, 1997a, 1997b] assumes zero initial dust concentration in the model atmosphere. Three-dimensional dust concentration fields available to the end of each day of the simulation are used as the initial data for the next 24-hour integration. Such organization of the computations allows obtaining an optimal model representation of the real weather developments. The experiment was initiated at March 13, 1998, 0000 UTC, and consisted of four consecutive 24-hour model runs.

[13] The Eta model is presently in use as one of the operational models at the National Center for Environmental Prediction (NCEP). The accuracy of the obtained weather forecasts is well studied [*Mesinger*, 1996]. Hence, we limit our discussion to the analysis of the event. For the verification purposes we use the Sea Level Pressure (SLP) patterns based on the data from the NCEP/National Center for Atmospheric Research (NCAR) Reanalysis Project (NNRP) archive (Figures 1a–1d) [*Kalnay et al.*, 1996]. A discussion of the real and the simulated SLP patterns is presented below. The use of the SLP patterns enables the understanding of the main weather developments of the event. The SLP patterns also enable an indirect evaluation of the corresponding surface wind characteristics. Patterns of the TOMS AI measurements of the four consecutive days of the March 13–16, 1998, period taken once a day at about 1100 LT, are presented in Figures 2a–2d. Simulated SLP distributions at 1200 UTC of each day of the March 13–16, 1998, period are given in Figures 3a–3d. The vertically integrated model dust loading patterns (g m^{-2}) are presented in Figures 4a–4d, with a shorter time interval of 12 hours starting from 1200 UTC March 14. Under the standard atmospheric conditions it is possible to assume the AI to be a function of the altitude z of the gravity center of the dust plume, the optical depth τ and the single scattering albedo ω of the aerosol. A linear relationship between the dust loading and AI values with a factor of about 2.0 may be used under such conditions [*Alpert et al.*, 2002].

4. Simulation Results and the Real Data

[14] The NNRP based SLP maps demonstrate a weak African cyclone already existent at 1200 UTC March 13, 1998 outside of the simulation area (25°N, 0°E, not shown). A dust plume with an AI maximum value of 1.5 found over Northern Africa at 1100 LT March 13, over the area between the coordinates 27°N–30°N, 15°E–20°E (Figure 2a), may not be associated with the cyclone.

[15] In 24 hours, i.e., to 1100 LT March 14, the plume shifted in the northeast direction and the AI values in its center slightly decreased (Figure 2b). The model simulated a dust plume with the dust loading of 4.5 g m^{-2} in the center (Figure 4a). A new cyclone was entering the forecast area from the west (Figure 3b). Comparison with the corresponding NNRP SLP pattern (Figure 1b) demonstrates quite a reasonable agreement between the reanalyzed and

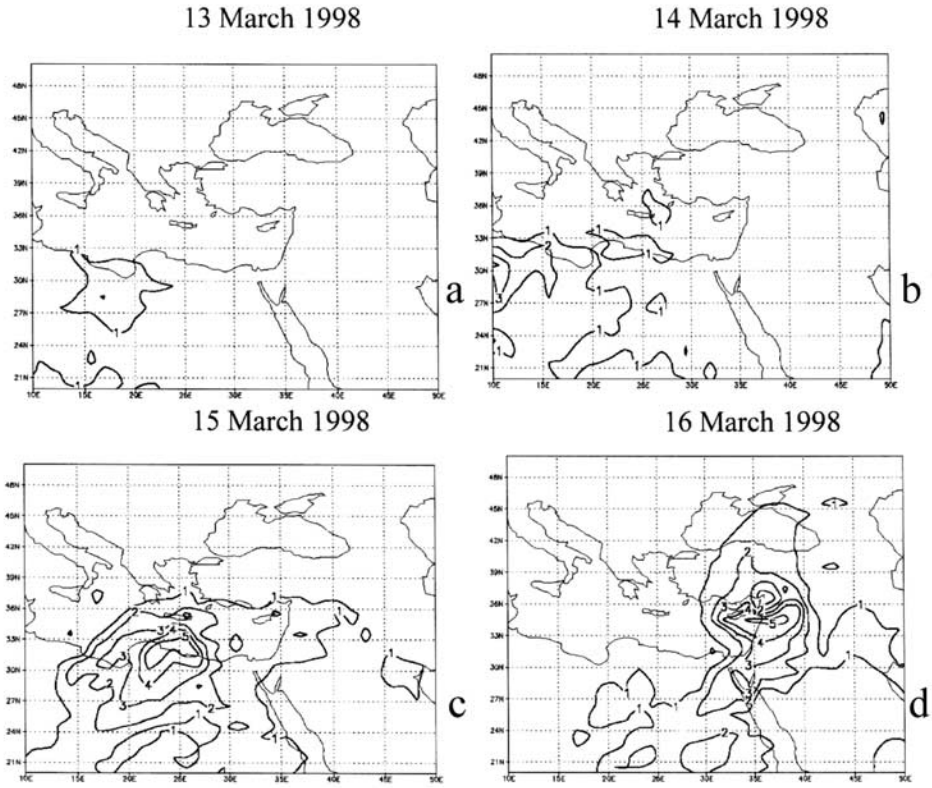

Figure 2. TOMS AI data at 1100 LT of (a) March 13, (b) March 14, (c) March 15, and (d) March 16, 1998 Contour interval is 1 AI unit.

simulated SLP patterns. The previous dust plume is found in Figure 2b over the area with central coordinates of about 35°N, 27°E. Another dust plume is located near the western boundary of the model domain, as presented in Figure 2b. The plume is associated with the new developing cyclone.

[16] The cyclone intensified during the following 24 hours. Its central pressure dropped to 995 hPa at 1200 UTC March 15 (Figure 1c). The model accurately described the process by producing SLP of 997 hPa at 1200 UTC March 15 (Figure 3c). At 1100 LT March 15 the main part of the real dust plume was located near to the Mediterranean coastal area (Figure 2c). A dramatic increase of the dust concentration took place before that moment: The maximum AI values in Figure 2c reached 5.0. The corresponding model-produced maximum dust loading has increased - up to 11 g m^{-2} (Figure 4c). In the end of the last day of the simulation (1200 UTC March 16) the real cyclone was located over the EM (Figure 1d). A deep dust plume (AI equal to 5) also located over the area was associated with the cyclone (Figure 2d). The positioning of the cyclone as well as its central pressure are accurately reproduced. The simulated dust loading value in the center of the plume over the EM was 12 g m^{-2} (Figure 4d).

5. Synoptic Analysis

[17] The TOMS AI data, which are often used as the main source for dust observations are available on the web with a 1° horizontal resolution. The 24-hour time resolution is not sufficient for synoptic analysis. The reasonable level of accuracy of the simulation allows application of its results for the following analysis. Our study is based on a combination of the real two-dimensional AI patterns, model-produced three-dimensional meteorological and dust concentration characteristics, as well as on the two-dimensionally determined dust loading patterns.

[18] According to the simulation results, the plume intensification coincided with that of the cyclone deepening. Separation of the dust particles to two zones around the cyclone center is well presented in Figures 4c and 4d.

[19] A more detailed illustration of the development at 1200 UTC March 15 is available in Figure 5. The dust loading (shaded) is complemented here by the isolines of the 850 hPa heights and temperatures (solid and dashed lines respectively). Two zones with increased dust concentration are simulated. The northern part of the plume is positioned in the vicinity of the warm front. It is characterized in the figure by relatively low dust loading values (4.0 g m^{-2}). The southern part of the plume is located in the area of the cold front, and is characterized by high (12 g m^{-2}) dust loading values. The result is in an agreement with dust plume conceptual model by *Karyampudy et al.* [1999].

[20] The three-dimensional time evolution of the dust plume is shown in Figures 6a–6j. The patterns here correspond to the plume development from 1200 UTC March 15 to 1500 UTC March 16 1998 with 3-hour time

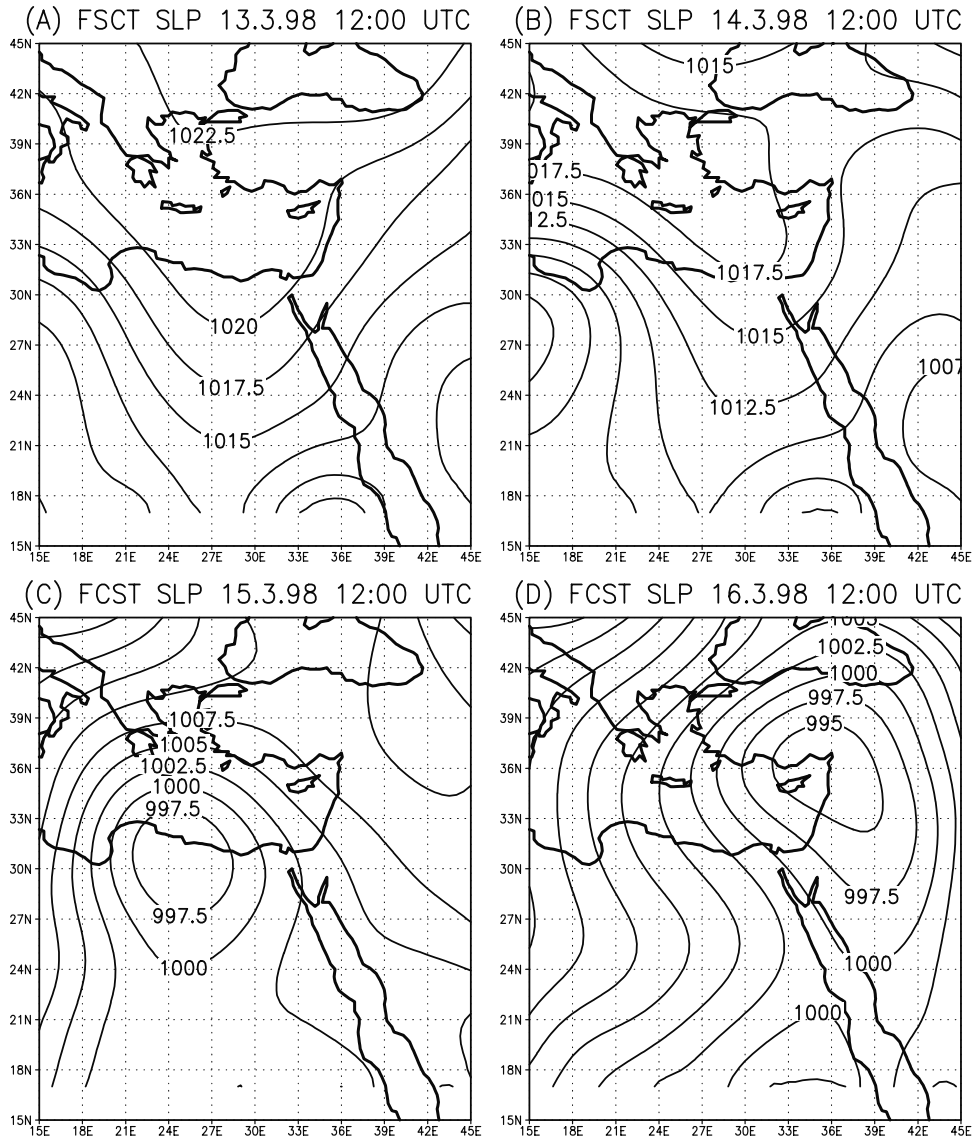

Figure 3. Model simulated SLP (hPa) at 1200 UTC of (a) 13 March, (b) 14 March, (c) 15 March, and (d) 16 March, 1998. Contour interval is 2.5 hPa.

interval. Only the areas with the dust concentration exceeding 1000 μg m^{-3} are presented. The air mass convergence in the mature cyclone evidently played a significant role in the dust plume evolution process. The role of the front related air mass updrafts in the process of development of the dust plume was also important. Formation of a two–layer dust plume during the process of its transport to the EM region appears to be a significant element of the development (Figures 6d–6j). Accurate simulation of the observed rain associated wet deposition process at about noon (Figures 6h–6j) may be indicated.

6. Vertical Structure of the Dust Plume

[21] Vertical profiles of the simulated dust concentration on 1200 UTC 15 March, 1998, at three locations (points 1, 3, and 5 in Figure 5) are presented in Figures 7a, 7c, and 7e. The simulated temperature and dew-point temperature profiles at these locations are presented in Figures 7b, 7d, and 7f. Point 1 is located in the cold front area over Northern Africa close to Sahara desert. The simulated dust layer was quite deep (4-km depth). The maximum dust concentration was simulated near the surface (about 5500 μg m^{-3}). According to the vertical distribution (Figure 7b) the aerosol layer was positioned under the lifted condensation level (LCL). The highest dust loading value (9–12 g m^{-2}) was simulated here.

[22] A similar vertical dust distribution characterized the situation at point 3 (Figures 7c and 7d). Values of the dust loading here were much lower - maximum of about 1.5–4.5 g m^{-2} (Figure 5). Again, practically all the dust content was located under the LCL positioned at 2-km height. The maximum dust concentration value was 1500 μg m^{-3}.

[23] The third point (Figures 7e and 7f) is located in the warm front area over the sea. Though the dust loading value here was almost the same as at location 3 (1.5–4.5 g m^{-2}), the dust particles are found here much above the located below 1 km LCL. The dust plume with small dust concen-

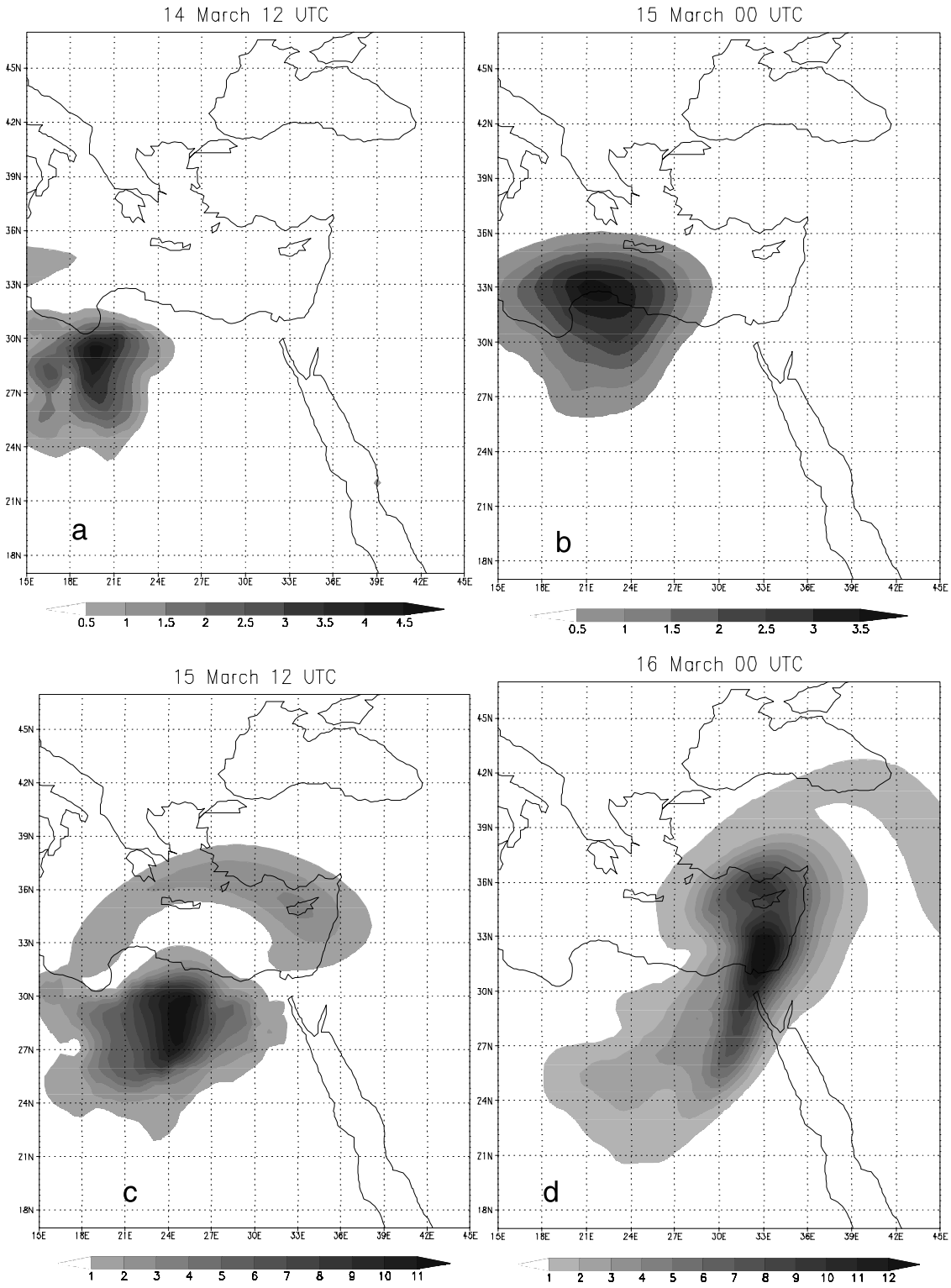

Figure 4. Model simulated dust loading (g m^{-2}) predicted for 24 hours to (a) 14 March 1200 UTC, (b) 15 March 0000 UTC, (c) 15 March 1200 UTC, and (d) 16 March 0000 UTC.

trations (about 500 μg m^{-3}) occupied the atmosphere up to an altitude of 9–10 km.

[24] The patterns illustrate a significant difference in the vertical distributions of the aerosol in the air masses over Africa and the Mediterranean Sea. Intensive moist convection processes over the Mediterranean Sea have destroyed the low–level inversion in the case under the analysis. The model stimulated the development of a very high layer occupied by the dust up to an altitude 9–10 km. Such vertical dust distribution is different from that typical for the continental regions over Africa. The highest dust loading value in the model run (16 g m^{-2}) was simulated at 1800

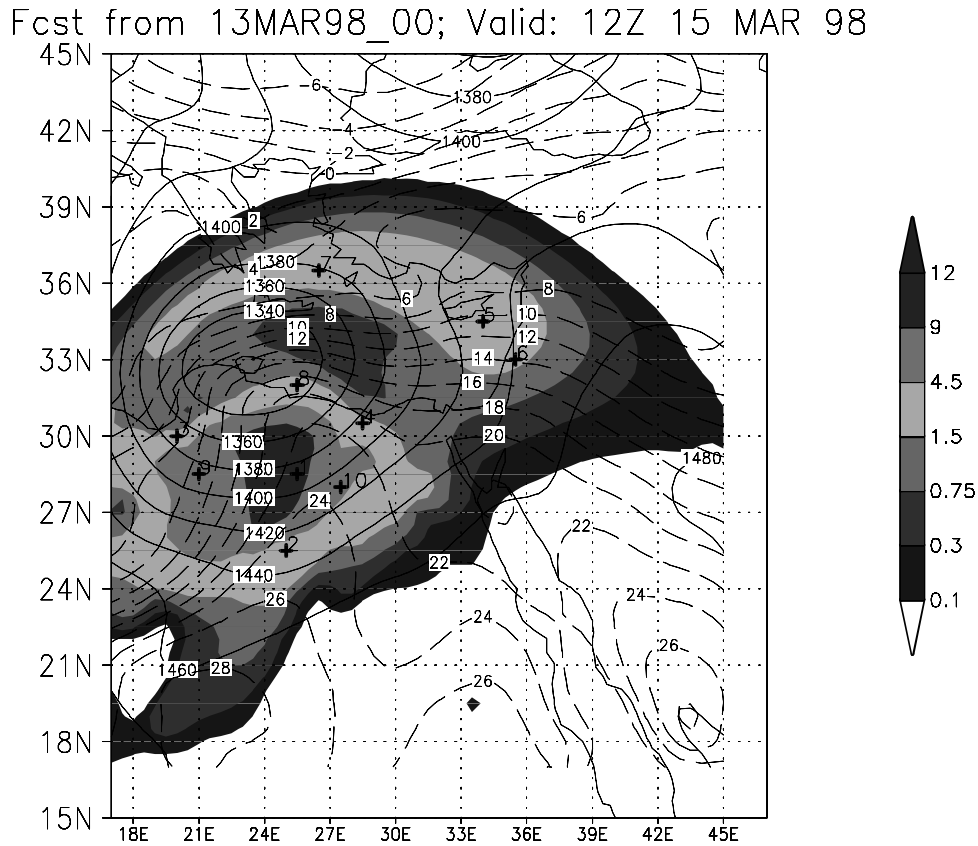

Figure 5. Results of 48-hour simulation at 0000 UTC 15 March, 1998; H-850 (solid lines), T-850 (dashed lines) and the dust loading (shading). Points 1, 2, and 3 are for locations, selected for analysis of the vertical distribution in Figure 7.

UTC March 15 over Northern Africa, 28°N, 28°E (Figure 8a). Vertical concentration of dust at this point (Figure 8b) demonstrated maximum dust concentration of about 7000 close to the surface. The plume's top is found at 4-km height. Time variation of the dust concentration at this point is illustrated by Figure 8c. The dust concentration increased at 0600 UTC March 15 and reached its maximum during the following 12 hours of the run (8000 $\mu g\ m^{-3}$). In the next 12 hours concentration decreased to 1000 $\mu g\ m^{-3}$ and increased again only at 1200 UTC March 17.

[25] The two-dimensional dust loading patterns are in good agreement with the TOMS AI data. At the same time it is evident that the forecast's accuracy is limited by the fact that the observation data on the three-dimensional dust distribution are presently not available. The existing satellite-based data (TOMS AI) provide only two-dimensionally determined characteristics. Additional efforts are required for using the data as a source of the information on the vertical aerosol distribution. Application of the model-simulated three-dimensional dust concentrations may be a possible solution. The presented above dust concentration profiles (Figures 7a, 7c, and 7e) illustrate the mesoscale variability of the dust vertical distribution in the cyclone.

7. Trajectory Analysis

[26] Though the dust distribution of the dust source areas in the model is known, determination of the area of origin of dust particles arriving to a particular region is a complicated task. Two factors are of importance. First, the space-time-variation of the soil moisture content affects the dust mobilization processes. Second, once mobilized, dust is transported to long distances. Accurate determination of the role of the time-space variation of the three-dimensional wind characteristics is not always straightforward.

[27] The area of the origin of the dust particles reaching a region may be determined with the help of the backward trajectory analysis. An advanced package for the three-dimensional trajectory calculation has been developed [*Wernli and Davies*, 1997]. The package allows three-dimensional (*x, y, p*) determination of the forward and backward trajectories based on the gridded model-predicted or analysis data. The procedure for objective identification of the different air streams consists of two steps: first, tracks of all air parcels are computed and, second, the ensembles of the trajectories are identified employing selected threshold criteria. Examples of application of the tool have been presented [e.g., *Tsidulko and Alpert*, 2001; *Krichak and Alpert*, 2000]. This method was applied to trace the dust particles arriving to Israel. Data from the model simulation were adapted. The use of the model-simulated dust concentrations allows taking into account the effects of the dust deposition processes. Backward trajectories from all grid points with dust concentrations exceeding 2300 $\mu g\ m^{-3}$, were computed.

[28] The 48-hour trajectories entering the target area with coordinates 31°N–27°N; 30°E–40°E area (shaded) in the

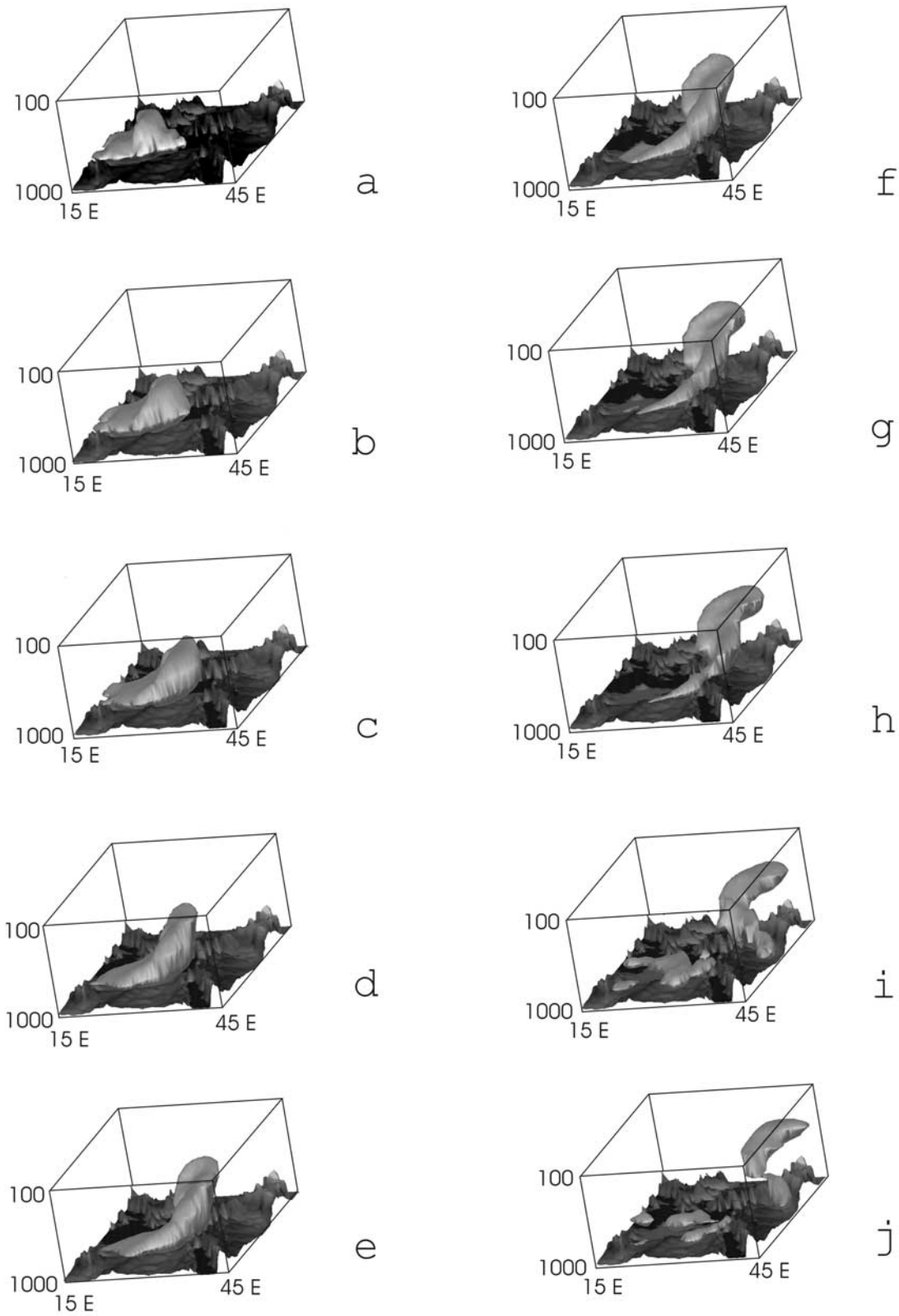

Figure 6. Three-dimensional representation of the model simulated process of the dust transport to the EM between 1200 UTC March 15 and 1500 UTC March 16, 1998. (a) 1200 UTC March 15. (b) 1500 UTC. (c) 1800 UTC. (d) 2100 UTC. (e) 0000 UTC. (f) 0300 UTC. (g) 0600 UTC. (h) 0900 UTC. (i) 1200 UTC. (j) 1500 UTC.

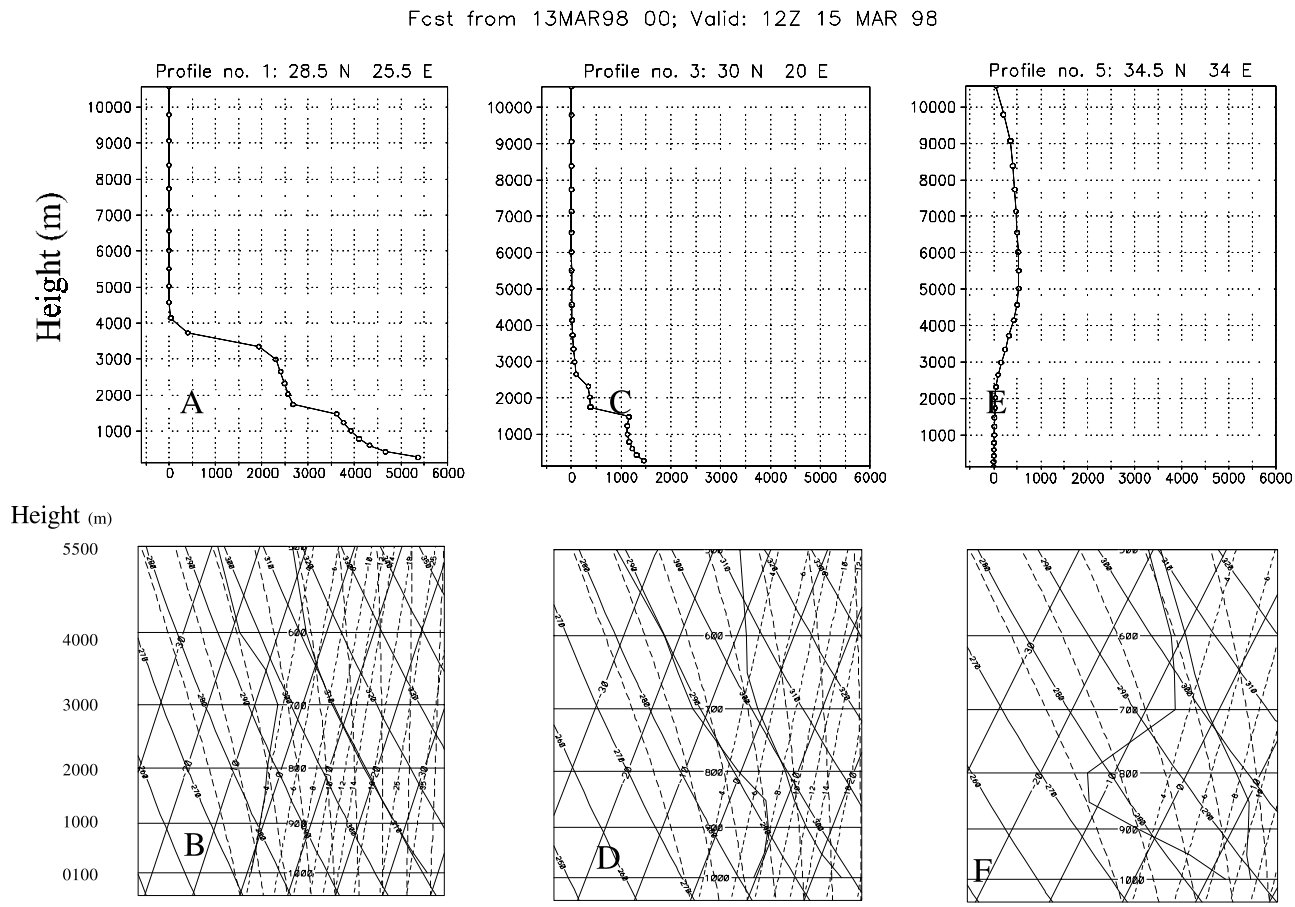

Figure 7. Vertical dust concentrations as well as temperature and dew point temperature profiles simulated for three locations indicated in Figure 5 at 1200 UTC 15 March, 1998. (a, c, and e) dust concentrations at locations 1, 3, and 5, respectively. (b, d, and f) temperature and dew point temperature profiles at the 1, 3, and 5 locations.

EM at 0600 UTC March 16, 1998, in the layer between 900 and 500 hPa are presented in Figure 9a. The variation of dust concentration along the cluster of the six obtained trajectories is given in Figure 9b. Two lines on this figure indicate the highest and lowest concentrations for the six trajectories. Simulated dust concentration was increasing from almost zero value to about 2500 $\mu g\ m^{-3}$ during 3-hr time interval from 0900 to 1200 UTC March 15, 1998. A slower increase of the concentration continued until 1800 UTC, until the maximum of about 5000 $\mu g\ m^{-3}$ was reached.

[29] The simulated displacement of the dust plume during the 24-hour time period from 0600 March 15 to 0600 UTC March 16, 1998, is presented in Figure 10a. An average route of the trajectories is also shown. Dots here indicate positioning of the corresponding air parcels with 3-hour time interval. The dust concentration maxima presented here were located in the lower troposphere (Figure 10b). At 0600 UTC March 15, a dust plume with maximum concentration about 300–500 $\mu g\ m^{-3}$ was simulated over the southern coast of the Sea (Figures 4b, 4c, and 9b). A large part of this developed in the cold front area plume reached the EM. According to the trajectory computations, this plume was slowly displacing along the trajectory. It is should be mentioned that the air mass was moving with a higher speed than that of the plume. It is likely that the air parcels moving along the trajectories overtook an already existing dust plume.

[30] According to the simulation, formation of the plume took place somewhat earlier. The vertical cross-section in Figure 10b illustrates the process. The dust enters the plume rising from the surface. Positioning of the areas with the maximum concentration of aerosol particles along the trajectories suggests that the formation of the dust plume with the exceptionally high dust concentration could be mainly associated with the strong air mass convergence due to the cyclone intensification.

8. Comparison With the Observed Surface Dust Concentration at Tel Aviv

[31] The model's ability to successfully reproduce the real developments may also be illustrated by comparing the simulated and measured surface dust concentration in Tel Aviv. According to *Alpert and Ganor* [2001] the measured surface dust concentration has increased from a typical non-dust-event value of about 30 $\mu g\ m^{-3}$ to the unusually high value of 8000 $\mu g\ m^{-3}$ during a short time interval from 0600 LT (0400 UTC) to 1100 LT (0900 UTC) March 16.

[32] The dust concentrations and dust loading simulated in Tel Aviv are given in Figure 11. At the surface, the

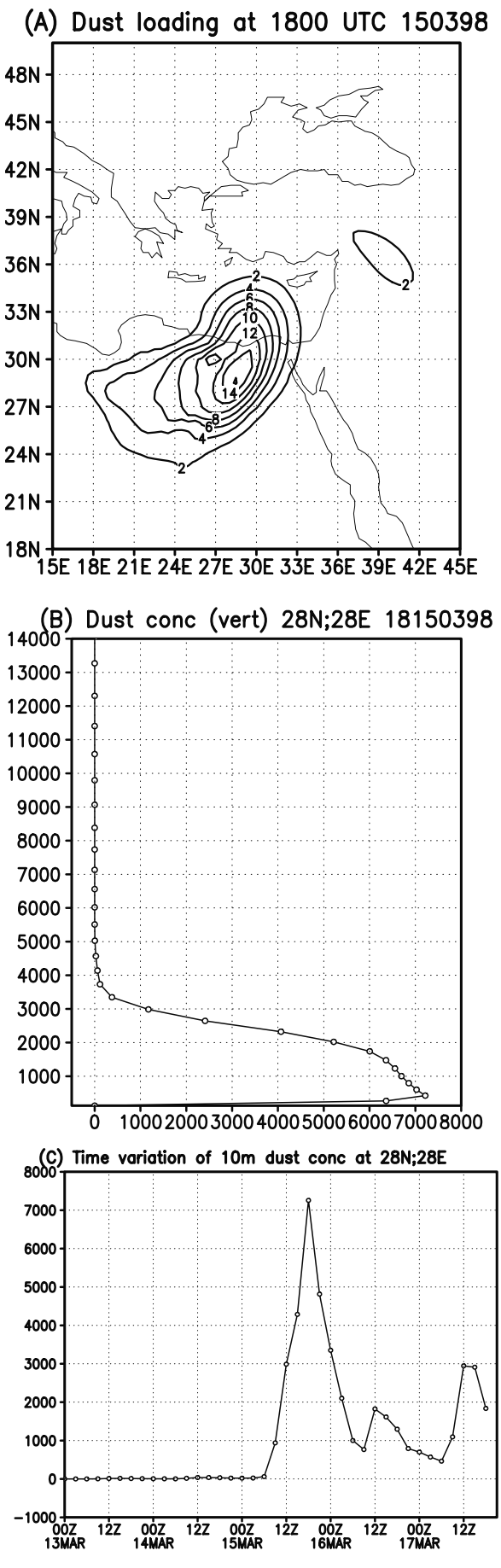

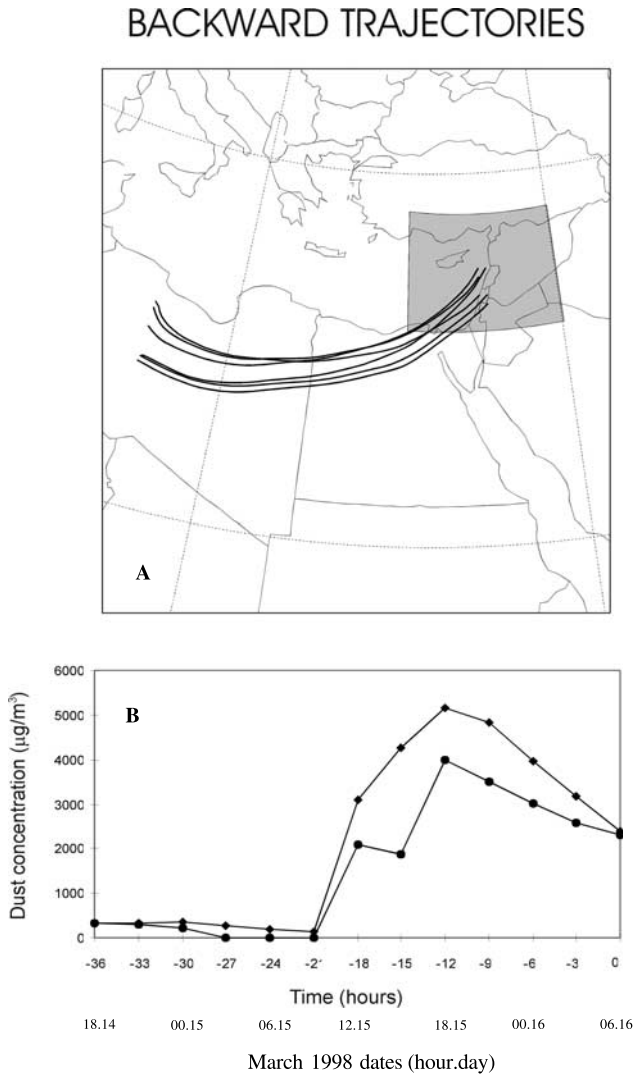

Figure 9. (a) The 48-hour back trajectories (16 March 0600 UTC to 14 March 0600 UTC) of air parcels with dust concentration greater 2300 μg m^{-3} entering the target area with the coordinates 30°N–40°N, 32°E–38°E (shaded) in the pressure layer of 900–500 hPa. (b) Variation of dust concentration along the cluster of the trajectories (real timing as well as the number of hours before 0600 UTC March 16 are indicated).

simulated process developed several hours earlier than the real one (Figure 11a). The concentration started increasing at about 2200 UTC March 15 (0000 LT March 16). The peak was predicted at 0600 UTC (0800 LT). The highest predicted dust concentration value however does not significantly differ from the observations (7500 μg m^{-3}). It may be pointed out that the dust loading maximum was simulated at an even earlier time moment (Figure 11b), about 0300 UTC (0500 LT) March 16.

Figure 8. (opposite) (a) Simulated dust loading, (b) vertical distribution, and (c) time variation of the dust concentration at 1800 UTC March 15, 1998, over the Northern Africa at 28°N, 28°E.

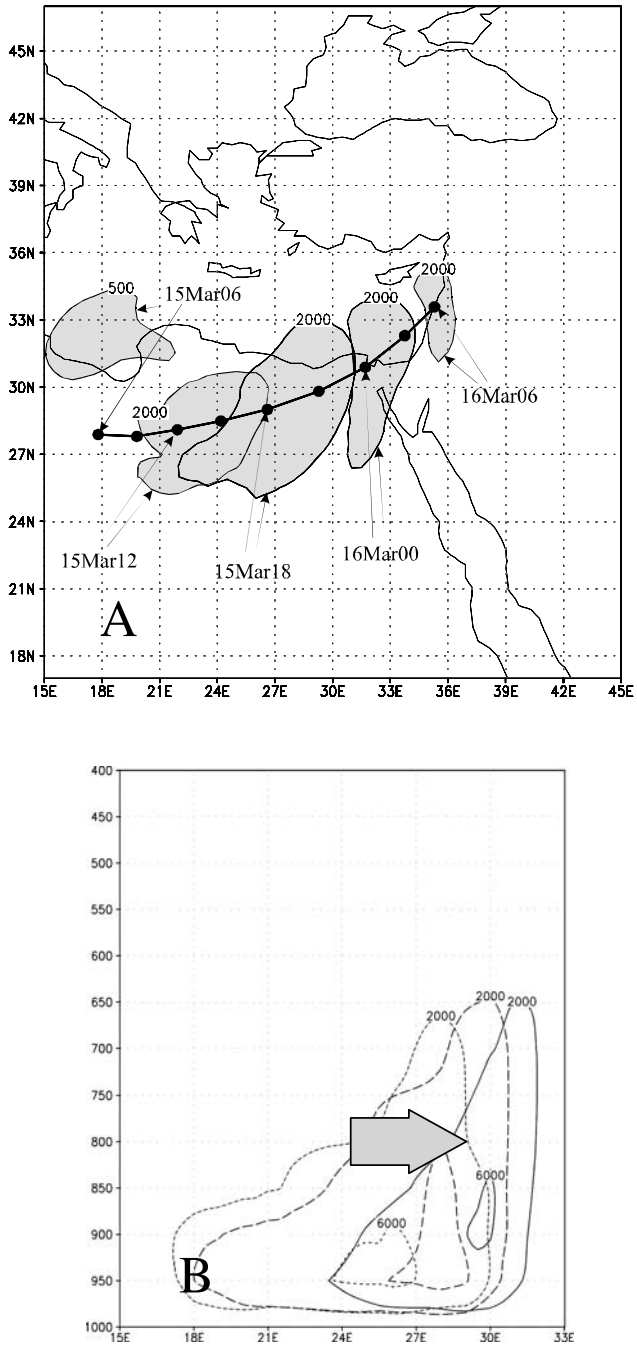

Figure 10. (a) Positioning of the dust plume during the period between 0600 UTC March 15 and 0600 UTC March 16 combined with the mean route of the air mass from Figure 8a. (b) Vertical cross-section of the dust concentration at 1200, 1500, and 1800 UTC 15 March, 1998, along 28.5°N latitude. The arrow indicates the layer with the main entering the dust plume trajectory.

9. Discussion and Summary

[33] A description of the plume development process may be suggested based on the analysis. Two stages of the process may be noted. The first stage was characterized by development and propagation of the dust plume over the Northern African region with a relatively mild dust loading of 3.0–4.5 g m^{-2}, about 1.0–2.0 AI units (Figures 2a, 4a, and 4b). The period ended prior to 1200 UTC March 15 when the maximum dust loading increased up to 11.0 g m^{-2} value (Figure 4c). The second stage was characterized by the transport of the intense dust plume to the EM area as well as an additional dust mobilization.

[34] The following scenario of the plume development may be suggested. The intensity of the dust storm appears to be a consequence of a joint action of several factors. Two main mechanisms were involved. The first was related to the dust mobilization process. A strong dust uptake took place on early March 15, 1998, in the process of the cyclone propagation over the dust source area in the Sahara Desert. The cyclone systems are often characterized by strong near-surface winds in the areas associated with intensive fronts. High temperature gradients in the frontal zone evidently contributed to the intensity of the squall line winds. The African cyclones are quite often characterized by strong winds of about 15-20 m s^{-1} [*Alpert and Ziv*, 1989; *Alpert and Ganor*, 1993; *Krichak and Alpert*, 2000]. Large quanti-

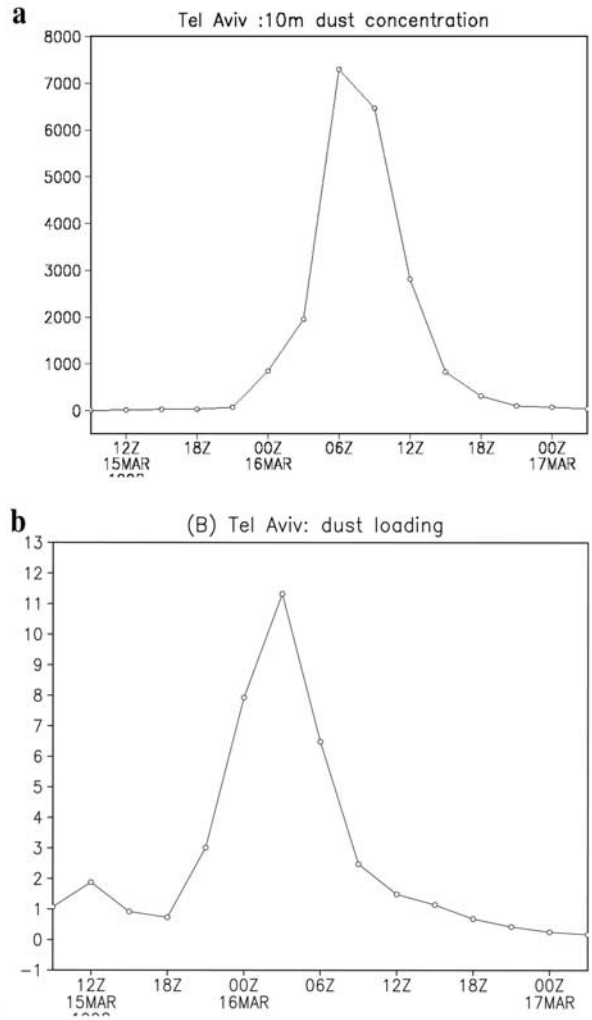

Figure 11. Simulated time variations at Tel Aviv between 1200 UTC March 15 and 0000 UTC March 17: (a) 10-m dust concentration (μg m^{-3}); (b) dust loading (g m^{-2}).

ties of the mineral dust aerosol particles were up-lifted into the lower atmosphere and were later transported over long distances into the eastern Mediterranean.

[35] The second important process was of a pure meteorological nature. The cyclone intensified by the noon of March 15 after its penetration into the Northern African coastal area. The wind structure of the developed mature cyclone and intensive air mass convergence played significant roles in the process. The intensification was associated with an increased dust convergence possibly enhanced by the moist air inflow to the cyclone. This process caused the abrupt and unusually intense increase of the dust concentration due to the intense convergence. Development of the two-layer structure of the dust plume could be one of the causes of the observed increase of the AI values, due to the increased sensitivity of the TOMS AI computation to the dust at the higher altitudes. Also, as pointed out by O. Torres (personal communication, 2001) the high AI-values may be partially explained by high reflectance from clouds beneath the upper-tropospheric dust.

[36] Accuracy of the model description of the March 1998 dust development over Northern Africa is demonstrated. The following directions of the possible model optimization may be listed. Accuracy of the real time dust predictions is quite sensitive to the dust initialization. Further improvement of the modeling system requires an improvement of the dust initialization procedure. An optimization of the described dust initialization procedure has recently been suggested by *Alpert et al.* [2002]. Additional model optimization is possible as a result of a more accurate determination of the dust source areas [*Ginoux and Torres*, 1999; *Israelevich et al.*, 2001]. Further improvements of the short-range dust predictions may be expected as a result of a more accurate initial determination of the meteorological characteristics and an increase of the model's space resolution. Inclusion of the radiation feedbacks into the radiation transfer computations as well as more accurate determination of the soil characteristics is also necessary. Use of a higher space resolution, more accurate description of the dust mobilization/transport/deposition/particle interaction processes as well as application of the multiparticle size approach [*Nickovic et al.*, 2001] may also allow an additional progress in the dust prediction.

[37] **Acknowledgments.** The study was supported by the Binational US-Israel Science Foundation (BSF) grant 97-00448. Partial support was provided by the DETECT-EC Project. The dust prediction system used in the study was adapted from the University of Athens. The system has been earlier developed at the framework of MEDUSE project funded from DG-XII of EU and the Greece-EU project SKIRON. The work of M. Tsidulko has been partially supported from the Israeli MEIDEX project. We thank H. Wernli for his assistance in adapting the trajectory analysis tool at Tel Aviv University. NCEP Reanalysis data provided by the NOAA-CIRES Climate Diagnostics Center, Boulder, Colorado, USA, from their Web site at http://www.cdc.noaa.gov/ were used in the study. Finally, we appreciate the constructive remarks by the reviewers.

References

Alpert, P., and E. Ganor, A jet stream associated heavy dust storm in the western Mediterranean, *J. Geophys. Res.*, *98*, 7339–7349, 1993.

Alpert, P., and E. Ganor, Sahara mineral dust measurements from TOMS: Comparison to surface observations over Middle East for the extreme dust storm, 14–17 March 1998, *J. Geophys. Res.*, *106*, 18,275–18,286, 2001.

Alpert, P., and B. Ziv, The Scharav cyclone: Observations and some theoretical considerations, *J. Geophys. Res.*, *94*, 18,495–18,514, 1989.

Alpert, P., Y. J. Kaufman, Y. Shay-El, D. Tanre, A. da Silva, S. Schubert, and J. H. Joseph, Quantification of dust-forced heating of the lower troposphere, *Nature*, *395*, 367–370, 1998.

Alpert, P., S. O. Krichak, M. Tsidulko, H. Shafir, and J. H. Joseph, A dust predication system with TOMS initialization, *Mon. Weather Rev.*, *130*, 2335–2345, 2002.

Betts, A., A new convective adjustment scheme, part E, Observational and theoretical basis, *Q. J. R. Meteorol. Soc.*, *112*, 677–691, 1986.

Cautenet, G., M. Leonard, and S. Cautenet, Thermal Impact of Saharan dust over land, 1, Simulation, *J. Appl. Meteorol.*, *30*, 166–180, 1992.

Chen, F., Z. Janjic, and K. Mitchell, Impact of atmospheric surface-layer parameterisations in the new land-surface scheme of the NCEP mesoscale Eta model, *Boundary Layer Meteorol.*, *85*, 391–421, 1997.

Fels, S. H., and N. D. Schwartzkopf, The simplified exchange approximation: A new method for radiative transfer calculations, *J. Atmos. Sci.*, *32*, 1475–1488, 1975.

Ginoux, P., and O. Torres, Global analysis of absorbing aerosol index derived from GOCART Model and TOMS data, paper presented at 2nd Gentner Symposium on Geoscience, Research Workshop on the Interactions between Chemistry, Physics and Dynamics in the Troposphere, SKIRON Project, Nazareth, Israel, October 24–29 1999.

Hsu, N. C., J. R. Herman, O. Torres, B. N. Holben, D. Tanre, T. F. Eck, A. Smirnov, B. Chatenet, and F. Lavenu, Comparisons of the TOMS aerosol index with sun photometer aerosol optical thickness: Results and applications, *J. Geophys. Res.*, *104*, 6269–6279, 1999.

Israelevich, P. L., Z. Levin, J. Joseph, and E. Ganor, Desert Aerosol Transport in the Mediterranean Region as Inferred from the TOMS Aerosol Index, *J. Geophys. Rev.*, *107*, 10.1029/2001JD002011, in press, 2001.

Janjic, J., The step-mountain Eta coordinate model: Further developments of the convection, viscous sub-layer and turbulence closure schemes, *Mon. Weather Rev.*, *122*, 927–945, 1994.

Janjic, Z. I., The step-mountain coordinate: Physical package, *Mon. Weather Rev.*, *118*, 1429–1443, 1990.

Kallos, G., et al., The regional weather forecasting system SKIRON: An Overview, paper presented at Symposium on Regional Weather Prediction on Parallel Computer Environments, Athens, 1997.

Kalnay, E., et al., The NCEP/NCAR 40-Year Reanalysis Project, *Bull. Am. Meteorol. Soc.*, *77*, 437–471, 1996.

Karyampudi, V. M., et al., Validation of the Saharan dust plume conceptual model using lidar, Meteosat and ECMWF data, *Bull. Am. Meteorol. Soc.*, *80*, 1045–1975, 1999.

Krichak, S. O., and P. Alpert, November 2, 1994 severe storms in the southeastern Mediterranean, *Atmos. Res.*, *53*, 45–62, 2000.

Krichak, S. O., M. Tsidulko, P. Alpert, A. Papadopoulos, O. Kakaliagou, and G. Kallos, Eta weather prediction system with the aerosol production/transport/ deposition at TAU, *MO/TD 942*, 5.29, World Meteorol. Org., Geneva, 1999.

Lacis, A. A., and J. E. Hansen, A parameterization for the absorption of solar radiation in the Earth's atmosphere, *J. Atmos. Sci.*, *31*, 118–133, 1974.

Marticorena, B., and G. Bergametti, Modeling of the atmospheric dust cycle, 1, Design of a soil-derived dust emission scheme, *J. Geophys. Res.*, *100*, 16,415–16,430, 1995.

Mesinger, F., Improvements in quantitative precipitation forecast with Eta regional model at the NCEP: The 48-hour upgrade, *Bull. Am. Meteorol. Soc.*, *77*, 2637–2647, 1996.

Mesinger, F., Z. I. Janjic, S. Nickovic, D. Gavrilov, and D. G. Deaven, The step-mountain coordinate: Model description and performance for cases of Alpine lee cyclogenesis and for a case of an Appalachian redevelopment, *Mon. Weather Rev.*, *116*, 1493–1518, 1988.

Nickovic, S., and S. Dobricic, A model for long-range transport of desert dust, *Mon. Weather Rev.*, *124*, 2537–2544, 1996.

Nickovic, S., D. Jovic, O. Kakaliagou, and G. Kallos, Production and long-range transport of desert dust in the Mediterranean region: Eta model simulations, paper presented at 22nd NATO/CCMS International Technical Meeting on Air Pollution Modeling and Its Applications, North Atlantic Treaty Org., Brussels, 1997a.

Nickovic, S., G. Kallos, O. Kakaliagou, and D. Jovic, Aerosol production/ / transport/deposition processes in the eta model desert dust cycle simulations, paper presented at Symposium on Regional Weather Prediction on Parallel Computer Environments, Athens, 1997b.

Nickovic, S., G. Kallos, A. Papadopoulous, and O. Kakaliagou, Model for prediction of desert dust cycle in the atmosphere, *J. Geophys. Res.*, *106*, 18,113–18,130, 2001.

Olson, J. S., A. Watts, and L. J. Allison, Major world ecosystem complexes ranked by carbon in live vegetation, *DNP-017*, Carbon Dioxide Inf. Cent., Oak Ridge Natl. Lab., Oak Ridge, Tenn., 1985.

Podgorny, I. A., W. Conant, V. Ramanathan, and S. K. Satheesh, Aerosol modulation of atmospheric and surface solar heating over the tropical Indian Ocean, *Tellus, Ser. B*, *52*, 947–958, 2000.

Prospero, J. M., P. Ginoux, O. Torres, and S. Nickolson, Environmental characterization of global sources of atmospheric soil dust derived from NIMBUS-7 TOMS absorbing aerosol products, *Rev. Geophys.*, *40*, doi:10.1029/2000RG000095, in press, 2002.

Rosenfeld, D., Y. Rudich, and R. Lahav, Desert dust suppressing precipitation: A possible desertification feedback loop, *Proc. Natl. Acad. Sci. USA*, *98*, 5975–5980, 2001.

Tsidulko, M., and P. Alpert, Synergism of upper-level potential vorticity and mountains in Genoa lee cyclogenesis: A numerical study, *Meteorol. Atmos. Phys.*, *78*, 261–285, 2001.

Wernli, H., and H. C. Davies, A Lagrangian-based analysis of extratropical Cyclones, I, The method and some applications, *Q. J. R. Meteorol. Soc.*, *123*, 467–489, 1997.

Westphal, D. L., O. B. Toon, and T. N. Carlson, A two-dimensional numerical investigation of the dynamics and microphysics of Saharan dust storms, *J. Geophys. Res.*, *92*, 3027–3049, 1987.

Zilitinkevich, S. S., Non-local turbulent transport: Pollution dispersion aspects of coherent structure of convective flows, in *Air Pollution III*, vol. I, *Air Pollution Theory and Simulation*, edited by H. Power, N. Moussiopoulos, and C. A. Brebbia, pp. 53–60, Comput. Mech., Boston, 1995.

P. Alpert and S. O. Krichak, Department of Biophysics and Planetary Sciences, Faculty of Exact Sciences, Tel Aviv University, Ramat Aviv, 69978 Tel Aviv, Israel. (pinhas@cyclone.tau.ac.il; shimon@cyclone.tau.ac.il)

O. Kakaliagou, G. Kallos, and A. Papadopoulos, School of Physics, Atmospheric Modeling and Weather Forecasting Group, University of Athens, University Campus Building PHYS-5, GR-15784 Athens, Greece. (olga@mg.uoa.gr; kallos@mg.uoa.gr; tasos@ncmr.gr)

M. Tsidulko, Coast Survey Development Laboratory, NOAA National Ocean Service, N/CS13, Room 7880, 1315 East-West Highway, Silver Spring, MD 20910, USA. (marina.tsidulko@noaa.gov)